Polycaprolactone nanofiber interspersed collagen type-I scaffold for bone regeneration: a unique injectable osteogenic scaffold

2013 Biomed. Mater. 8 045011

(http://iopscience.iop.org/1748-605X/8/4/045011)

Biomed. Mater. **8** (2013) 045011 (11pp) doi:10.1088/1748-6041/8/4/045011

Polycaprolactone nanofiber interspersed collagen type-I scaffold for bone regeneration: a unique injectable osteogenic scaffold

Nuray Baylan[1], Samerna Bhat[2], Maggie Ditto[1], Joseph G Lawrence[1], Beata Lecka-Czernik[2,3,4] and Eda Yildirim-Ayan[1,2,5]

[1] Department of Bioengineering, College of Engineering, University of Toledo, Toledo, OH 43606, USA
[2] Department of Orthopaedic Surgery, University of Toledo Medical Center, Toledo, OH 43614, USA
[3] Department of Physiology and Pharmacology, University of Toledo Medical Center, Toledo, OH 43614, USA
[4] Center for Diabetes and Endocrine Research, University of Toledo Medical Center, Toledo, OH 43614, USA

E-mail: eda.yildirimayan@utoledo.edu

Received 26 February 2013
Accepted for publication 17 May 2013
Published 27 June 2013
Online at stacks.iop.org/BMM/8/045011

Abstract

There is an increasing demand for an injectable cell coupled three-dimensional (3D) scaffold to be used as bone fracture augmentation material. To address this demand, a novel injectable osteogenic scaffold called PN-COL was developed using cells, a natural polymer (collagen type-I), and a synthetic polymer (polycaprolactone (PCL)). The injectable nanofibrous PN-COL is created by interspersing PCL nanofibers within pre-osteoblast cell embedded collagen type-I. This simple yet novel and powerful approach provides a great benefit as an injectable bone scaffold over other non-living bone fracture stabilization polymers, such as polymethylmethacrylate and calcium content resin-based materials. The advantages of injectability and the biomimicry of collagen was coupled with the structural support of PCL nanofibers, to create cell encapsulated injectable 3D bone scaffolds with intricate porous internal architecture and high osteoconductivity. The effects of PCL nanofiber inclusion within the cell encapsulated collagen matrix has been evaluated for scaffold size retention and osteocompatibility, as well as for MC3T3-E1 cells osteogenic activity. The structural analysis of novel bioactive material proved that the material is chemically stable enough in an aqueous solution for an extended period of time without using crosslinking reagents, but it is also viscous enough to be injected through a syringe needle. Data from long-term *in vitro* proliferation and differentiation data suggests that novel PN-COL scaffolds promote the osteoblast proliferation, phenotype expression, and formation of mineralized matrix. This study demonstrates for the first time the feasibility of creating a structurally competent, injectable, cell embedded bone tissue scaffold. Furthermore, the results demonstrate the advantages of mimicking the hierarchical architecture of native bone with nano- and micro-size formation through introducing PCL nanofibers within macron-size collagen fibers and in promoting osteoblast phenotype progression for bone regeneration.

(Some figures may appear in colour only in the online journal)

[5] Author to whom any correspondence should be addressed.

1. Introduction

Irregular-shaped bone fractures, mostly seen in osteoporotic bone fractures cases, have been stabilized using injectable materials such as polymethylmethacrylate (PMMA) (bone cement) and calcium content resin-based materials due to their minimally invasive administration [1]. However, these materials all fall short of clinical expectations for reasons such as the exothermic polymerization process, mismatched mechanical properties (high modulus) with osteoporotic bone [2, 3] and the lack of regenerative potential [4–8]. There is a great demand for a new generation injectable biomaterial possessing proper biological, mechanical and structural properties to host cells and to regenerate bones at the injected area while stabilizing the fracture. New generation injectable orthobiologic material may have the potential to induce bone restoration while releasing osteoinductive factors in a controllable fashion and thus holding a newly formed bone matrix.

Collagen is an excellent material for injectable and implantable scaffolds to regenerate bone because of its permeability, *in vivo* stability, and inherent biochemical properties [7, 9–11]. Numerous studies conducted with collagen sponges, collagen membranes, and electrospun collagen fibers have shown that cells seeded on such scaffolds can differentiate and deposit abundant extracellular matrices throughout the scaffolds [9–11]. However, collagen by itself cannot serve as a bone-filler because it has poor mechanical properties and a high degradation rate for bone tissue. Therefore, collagen cannot provide long-term structural support for load-bearing conditions [12].

In order to overcome these limitations, collagen has been mixed with synthetic biocompatible polymers such as polycaprolactone (PCL) [12, 13]. PCL is a FDA approved biocompatible material with optimum mechanical and degradation properties suitable for bone tissue [14, 15]. As a result, PCL–collagen composite scaffolds in different forms including sponge, 3D well-defined scaffold, electrospun fiber materials, and membrane form have been used both in *in vitro* and *in vivo* studies for bone regeneration [12, 13, 16–18].

The electrospining of collagen and collagen–PCL blends is a common technique to produce a 3D nanofibrous collagen-based scaffold. However, electrospining processes may create conformational changes in the structure of the collagen [19]. Previous studies have found that during electrospining processes water-insoluble collagen becomes water soluble due to high electric field exposure and highly volatile fluoroalcohol (used for dissolving collagen and collagen/polymer) exposure [19–25]. It has also been demonstrated that up to 45% of collagen can be lost during the electrospining process [19, 26]. In addition, electrospun collagen and collagen–PCL scaffolds need stabilization to preserve the collagen fiber formation. However, the stabilization is generally conducted with toxic crosslinking agents including glutaraldehyde, and N-(3-dimethylaminopropyl)-N′-ethylcarbodiimide hydrochloride [12, 21, 27, 28].

Another common technique to create composite collagen–PCL scaffold is merging the rapid prototyping technique with collagen deposition. In these studies, PCL scaffolds were created in a layer-by-layer fashion to create a three-dimensional (3D) matrix, then collagen is generally deposited with or without cells onto the 3D PCL scaffold. In this technique, no harsh chemicals are used to dissolve the PCL since the PCL scaffold manufacturing was based on rapid prototyping techniques. For instance, Ahn *et al* [18] studied the effect of PCL–collagen hybrid scaffolds on the cellular activities of osteoblast-like cells (MG63). The 3D interdigitated micro-structured PCL–collagen scaffolds were created using melt-plotting and a low temperature plate. Then the cells were seeded on a hybrid PCL–collagen scaffold to run an *in vitro* study. The *in vitro* study showed that, MG63 cells exhibited higher cell-seeding efficiency, cell-viability, and calcium deposition on a PCL–collagen scaffold compared to those of pure PCL scaffolds. The results were attributed to the increased mechanical stiffness due to PCL and increased bioactivity of the hybrid scaffold due to collagen. Lee *et al* [13] also created hybrid PCL–collagen scaffolds from PCL microstrands and electrospun collagen for bone tissue regeneration. They followed the layer-by-layer manufacturing technique to create their hybrid scaffold. Basically, PCL microstrands were created in a designed fashion and collagen was electrospun on this layer, then a second layer of PCL microstrands were deposited again on the electrospun collagen. They seeded osteoblast-like cells (MG63) onto a hybrid PCL–collagen scaffold to assess the osteoconductivity of the scaffolds. Their results showed that PCL–collagen scaffolds promoted the MG63 cell proliferation, adhesion, and expression of bone-associated genes. Richert *et al* [29] created a PCL–collagen hydrogel construct seeded with mesenchymal stem cells (MSCs) for bone regeneration. The scaffold consisted of two parts. The first part is the 3D PCL scaffold manufactured with a fused deposition system and the second part is the collagen hydrogel with embedded MSCs. To create a composite PCL–collagen scaffold, MSCs loaded with a collagen gel were dropped on to a 3D collagen scaffold. Their results showed that the PCL–collagen scaffold could promote an osteogenic differentiation pathway for MSCs. Although no harsh chemicals were used to dissolve the PCL and collagen in these scaffolds, the introduction of these composite PCL–collagen scaffolds in to the body of interest still requires an invasive surgery.

In the light of the above discussion, the current study is aimed at creating a next generation, injectable biomaterial as a bone filler containing pre-osteoblast cells, nanofibrous PCL synthetic polymers and collagen type-I natural polymers. This will mimic the micro/nano-hierarchal architecture of the native bone and will create a 3D environment for bone cell-ingrowth, proliferation and differentiation. In this study, the advantages of injectability and biomimicry of collagen were coupled with PCL nanofibers, to create cell encapsulated injectable 3D bone scaffolds with intricate porous internal architecture and high osteoconductivity. Nanofibrous PCL–collagen (PN-COL) scaffolds were manufactured with varying PCL concentrations of 0% (w/v), 1% (w/v), and 6% (w/v) to evaluate the injectable PN-COL scaffolds with respect to their physiochemical, morphological, biological properties.

Specifically, we investigated the effect of the PCL nanofiber concentration within collagen on a scaffold's architectural and chemical properties, and the osteogenic activity of the scaffold. In particular, we investigated the changes on scaffold's structural stability, chemical composition, internal architecture, on pre-osteoblast's cell morphology, viability, proliferation, and on osteogenic activity including alkaline phosphates activity, matrix mineralization, and the total matrix protein production following PCL nanofibers incorporation within collagen type-I.

2. Materials and methods

2.1. Injectable osteogenic scaffold fabrication

The biomaterial composite PCL nanofibers interspersed with collagen (PN-COL) was obtained by incorporating PCL nanofibers within collagen type-I (BD Science, USA) with different ratios. A detailed description of the manufacture of the injectable PN-COL scaffold is given below.

PCL nanofiber fabrication. PCL (Mw = 45 000, Sigma-Aldrich) nanofibers were obtained by electrospining techniques. PCL was dissolved in a solvent mixture with a volume ratio of 7:3 chloroform/methanol (v/v) by gently stirring at room temperature for 24 h to form a homogenous solution. A 12% (w/v) PCL solution was delivered via a syringe pump (New Era Pump Systems, Inc.) fitted with a 20-gauge needle at a flow rate of 750 μl h^{-1}. PCL nanofibers were fabricated using a positive voltage of 20 kV applied between the needle and a grounded aluminum foil plate separated by a distance of 12 cm using a high voltage power supply (ES30 P, Gamma High Voltage). All the electrospining processes were carried out under ambient conditions of 24 $\pm$ 3 °C temperature with 50 $\pm$ 5% relative humidity for 1 h. The fibrous meshes on the aluminum foil plate were collected and dried in the desiccator for 72 h to remove residual organic solvent and moisture. The PCL nanofiber mats were then homogenized using a high speed homogenizer (Ultra-Turrax, IKA Works, Inc.). Prior to mixing the PCL nanofibers with the collagen type-I solution, PCL nanofibers were functionalized with an oxygen-based plasma for 3 min to introduce oxygen-containing functional groups on nanofibers to reduce its hydrophobicity as previously described [14, 16].

Collagen solution neutralization and PCL nanofiber induction. The collagen type-I solution (BD Bioscience; USA) had a concentration of 3.61 mg ml^{-1} with a pH of ∼3–4. It should be noted that the collagen type-I came from a vendor in a solution form. Since the collagen type-I was already in an aqueous form; there was no need to dissolve it with a solvent. This collagen solution was diluted to 2.5 mg ml^{-1} and pH neutralized to 7.0 with the help of chilled 1M sodium hydroxide, phosphate buffered saline (PBS) and deionized water. The plasma-treated PCL nanofibers were then mixed with the prepared collagen solution with a ratio of 1% (w/v) and 6% (w/v) to obtain an injectable composite PN-COL scaffold. This composite scaffold solution was stored at 4 °C to prevent collagen polymerization until mixing with cells for *in vitro* studies.

2.2. Structural stability analysis of PN-COL composite scaffold

The size retention of PN-COL scaffolds with varying PCL concentrations (0%, 1%, and 6% (w/v)) were calculated following a 14 day culture at incubator conditions to understand the effect of increased PCL concentration within a PN-COL scaffold in scaffold size retention. The changes in scaffold size were quantified using an optical image of the scaffolds. From the images, a size retention percentage calculation was obtained by dividing the scaffold size at day 14 to the scaffold size at day 0. For the original size calculation at day 0, the bottom surface area of a well in a 48-well plate was used because at day 0, deposited material covered the bottom of the well in all experimental groups. For size measurements at day 0 and day 14, optical images of the samples were taken by a camera after washing the samples twice with PBS. The optical images were then uploaded to Image-J software from NIH for area calculation. Four area measurements were done for each sample ($n = 4$).

2.3. Morphology and chemical composition analysis of PN-COL composite scaffold

The morphological changes due to PCL nanofiber induction to the collagen scaffold were examined by scanning electron microscopy (SEM) (Quanta 3D FEG). Prior to SEM analysis, PN-COL scaffolds were fixed with 4% paraformaldehyde solution (Sigma Aldrich; USA) for 1 h, and then post-fixed in 1% (v/v) osmium tetroxide diluted with Sorensen's buffer to preserve the collagen fibrils and to enhance the image quality. After fixation, the samples were rinsed twice with PBS, and subsequently dehydrated in increasing concentrations of ethanol from 30% to 100% and ethanol/ hexamethyldisilazane (HMDS) solutions from 30% to 100 % for 15 min each. Further, the samples were air-dried under the chemical hood over-night to evaporate the residual ethanol and HMDS. The dried samples were then sputter coated with a thin layer of gold to avoid charging.

The chemical changes due to the incorporation of PCL nanofibers in the collagen type-I solution were quantified by Fourier transform infrared spectroscopy (FTIR). The FTIR spectra of the samples were collected using a germanium ATR (attenuated total reflection) crystal in the Digilab Excalibur FTS 4000 FTIR spectrometer with UMA 600 microscope. The spectra for a collagen scaffold (0% w/v) and PN-COL scaffolds with 1% (w/v) and 6% (w/v) were obtained by accumulating 256 scans with a resolution of 4 cm^{-1} in the range of 800–4000 cm^{-1}.

2.4. Long-term in vitro evaluation of injectable PN-COL composite scaffolds

A long-term *in vitro* study (21 days) was designed with pre-osteoblast cells encapsulated within PN-COL injectable scaffolds to investigate the changes in cell morphology, viability, proliferation, and osteogenic activity including alkaline phosphates activity, matrix mineralization, and total

matrix protein production within varying PCL nanofibers concentrations in composite PN-COL scaffolds.

The pre-osteoblastic cells, MC3T3-E1 (ATCC, CRL-2593; USA) between passages numbered two and four were used. Cells were populated in a complete medium of α-minimum essential medium (α-MEM) (Life Technologies, USA) supplemented with 1% antibiotics (Life Technologies, USA), 10% (v/v) fetal bovine serum (FBS) (Gibco; USA) in an incubator maintained at 37 °C and 5% CO_2. Three days prior to cell incorporation into a scaffold, cells were cultured with an osteogenic media prepared by adding osteogenic factors including 10 mM β-glycerophosphate and 50 μg mL^{-1} ascorbic acid (Sigma-Aldrich, USA) to the complete media. Pre-incubated cells were then encapsulated within a sterile collagen-PCL scaffold with a density of 1×10^6 cells mL^{-1} and placed inside an incubator at 37 °C for an hour to initiate the collagen polymerization. Collagen is a biomolecule consisting of a homogenous collection of thin fibers. These fibers become cross-linked when conditions are adjusted to near physiological values (pH of 6.5–8.5 and temperature 20–37.5 °C). In the literature, the crosslinking of collagen fibers is called 'collagen gelation' or 'collagen matrix polymerization' [30–32]. Following polymerization for 1 h, the fresh complete medium was added to each sample. Cell encapsulated polymerized PN-COL scaffolds were moved to the incubator until the characterization day.

The *encapsulated cell proliferation* within the PN-COL scaffold was examined using non-toxic alamarBlue (aB) assay (Biosource International, USA) at days 14 and 21. For each group four samples were used ($n = 4$). On the day of characterization, 10% (v/v) of aB assay solution was added to each sample and allowed to incubate for 6 h at incubator conditions. Following the incubation, 250 μL solution of colored product was taken out from the wells and put into a 48 well-plate to measure the fluorescence intensity using a microplate fluorometer (Wallac 1420, USA) at 545 nm excitation and 585 nm emission wavelengths.

The *encapsulated cell viability* within the PN-COL scaffold was assessed quantitatively and qualitatively using Live/Dead assay (Life Technologies, USA) at day 14. Confocal images of live and dead cells within 3D scaffolds were taken following incubation with Live/Dead assay for these analyses. Briefly, for confocal images, on characterization day, samples were first washed twice with PBS for 5 min and then incubated in a Live/dead assay for 30 min. The assay was composed of a 1:4 concentration ratio of calcein AM for labeling live cells and ethidium homodimer-1 for labeling dead cells in PBS. After incubation, the samples were fixed using 4% paraformaldehyde (Sigma Aldrich, USA) in PBS for 30 min. Post fixation, the samples were washed three times with PBS for 15 min. The samples were then stored at 4 °C until they were imaged using a Leica TCS SPE Confocal microscope with multiphoton. Calcein AM was visualized using a 488 nm laser and an emission spectrum of 491 to 545 nm. Ethidium homodimer-1 was visualized using a 568 nm laser and an emission spectrum of 590 to 685 nm. For quantitate analysis, cell counting was completed on the ~40 μm thick images. Prior to counting cells, the images were divided into a 5×5 grids to facilitate the counting. The numbers of live and dead cells were then counted in each grid square. The live and dead cell counts were summed and the percent viability was calculated as the ratio of live cells to total cells.

The *alkaline phosphatase (ALP) activity* was evaluated on the PN-COL composite scaffold with varying PCL concentrations of 0%, 1%, and 6 (w/v) at day 14 using alkaline phosphatase colorimetric assay (Abcam, USA). For each group four samples were used ($n = 4$). The assay measures p-nitrophenol (pNP) converted from p-nitrophenyl phosphate in the presence of ALP. The rate of pNP production is linearly proportional to the ALP activity. Prior to ALP analysis, the cells inside the collagen–PCL scaffold were liberated by incubating the scaffolds with a 0.2% (w/v) collagenase type-I solution (Life Technologies, USA) with complete media for 1 h at 37 °C in a shaking water bath. Then, the whole solution was centrifuged to isolate the cell pellet for the ALP measurement. The ALP assay was performed based on the manufacturer's protocol (ab83369, Abcam®). The pNP production was determined by measuring the absorbance at 405 nm using a microplate reader (SOFTmax Pro). To convert the measured absorbance to pNP value, a standard curve was established using a serial dilution of pNP according to the manufacturer's protocol.

The *matrix mineralization and the progression of calcium deposition* within and on the PN-COL composite scaffolds were quantified by Alizarin Red assay (Millipore, catalog # ECM815; USA) and were visualized by SEM imaging at day 14 and day 21. For each group four samples were used ($n = 4$). Constructs containing cells were digested using 0.2% (w/v) collagenase solution with complete media for an hour at 37 °C. Following digestion, the whole solution was incubated further with 0.05% (w/v) trichloroacetic acid solution to release the mineralized matrix on the PCL nanofibers. The amount of mineralized matrix was then measured according to the manufacturer's protocol with a microplate reader (SOFTmax Pro) at an absorbance of 405 nm. The optical density value obtained from the measurement is linearly correlated with the amount of mineralized matrix. For visualizing the mineralized matrix, SEM imaging protocol was followed (section 2.3).

To identify the *total protein production* of cells on collagen and PN-COL scaffolds, the BCA Protein Assay (Pierce Protein Biology Product; USA) was used. Prior to the assays, cells were liberated from the collagen matrix by incubating them with (%0.02 w/v) collagenase solution for 1 h at 37 °C and lysed to release the proteins. The manufacturer's protocol was followed to conduct the assay. Bovine serum albumin (BSA) was used as a protein standard. The results gave a quantitative measure of matrix protein production in a PN-COL composite scaffold.

2.5. Statistical analysis

Statistical analysis was performed using SPSS software version 10.2. All the data were expressed as the mean ± standard deviation. Differences between groups were analyzed by investigation of variance (ANOVA) with the LSD post hoc test. In the proliferation result evaluation two-sample

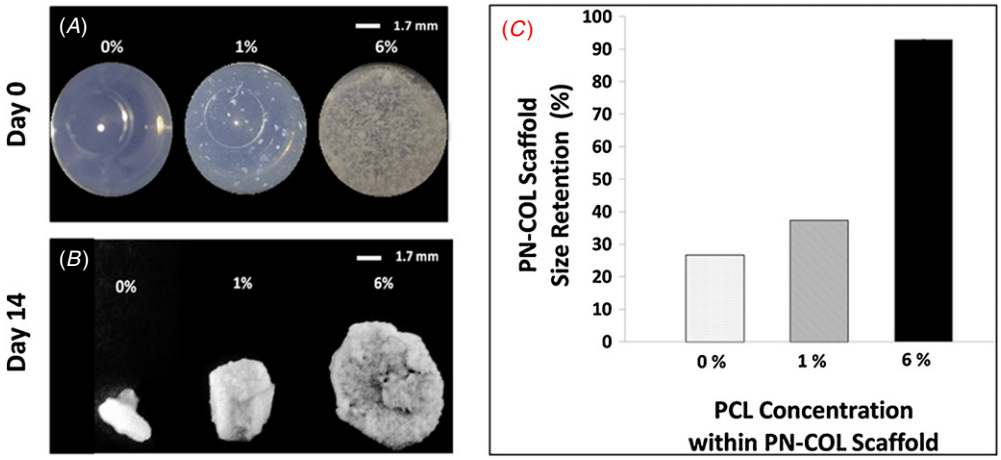

Figure 1. (*A*) Optical images of the PN-COL scaffolds with 0%, 1% and 6% (w/v) PCL at day 0. (*B*) Optical images of the PN-COL scaffolds with 0%, 1% and 6% (w/v) PCL at day 14. (*C*) Graph showing changes in scaffold size retention percentage with increased PCL concentration within PN-COL scaffolds.

T-tests were conducted to identify and to clarify the difference between cell numbers within sample groups at day 14 and day 21. To identify and to clarify the statistical significance of PCL concentration on cell proliferation one-way ANOVA was run. The paired Student's *t*-test was performed to analyze the difference for ALP activity, mineralization and total protein production between 1% (w/v) PN-COL and 6% (w/v) PN-COL scaffold. Differences were considered as significant when $p < 0.05$.

3. Results

3.1. PCL nanofiber concentration within PN-COL mediates scaffold structural stability

It is well-known that the collagen coupled with cells cannot retain its original size due to contraction [33, 34]. The changes in scaffold size were studied since the size retention of injectable bone filler within the injected area is very important for successful bone fracture stabilization. In this study, the size retention of PN-COL scaffolds with varying PCL concentrations (0%, 1%, and 6% (w/v)) were calculated following 14 day cell culturing at incubator conditions (37 °C). The scaffold size retention percentage was then calculated by dividing the scaffold size at day 14 by the scaffold size at day 0. Figure 1 shows the optical images of scaffolds on day 0 and day 14, and also shows the graph on changes in scaffold size retention percentage with increased PCL concentration within PN-COL scaffolds. The results suggested that scaffold size retention increased with the increased PCL nanofiber concentration within the PN-COL composite matrix. The PN-COL scaffold with 6% (w/v) PCL concentration was able to preserve the initial injected volume up to 95% (figure 1(*C*)) while the size retention percentage was only 38% for 1% (w/v) PN-COL preserved. For pure collagen scaffolds (0% PN-COL) the dimension shrinkage was significant. Following 14 days of culture, the size retention percentage was only 25% for 0% (w/v) PN-COL scaffolds.

3.2. PCL nanofiber concentration within PN-COL mediates scaffold morphology and chemical composition

Tissue scaffold morphology and cell–biomaterial interaction sets the stage for cell attachment and also affects the cell phenotype and functions [14, 35, 36]. Therefore, it is important to understand the effect of PCL nanofiber introduction within collagen scaffolds in respect to scaffold morphology.

Figure 2 shows the SEM image of injectable PN-COL scaffold morphology with varying PCL nanofiber concentrations with lower and higher magnification. The images suggest that with increased PCL nanofiber concentrations, the scaffolds' morphologies change dramatically. The fiber sizes were decreased with the increased PCL incorporation. The introduction of PCL nanofibers within collagen provided a large surface-area-to-volume ratio for cell attachment and proliferation. For a pure collagen scaffold (0% (w/v) PCL within scaffold), the thickness of the collagen fibers was around 500 nm. Following 1% (w/v) PCL nanofiber and 6% (w/v) PCL nanofiber induction to the collagen, the fiber sizes inside the scaffold reduced to 100 and to 5 nm, respectively. The introduction of PCL nanofibers within collagen provided a large surface-area-to-volume ratio for cell attachment and proliferation.

Changes in chemical composition with the introduction of PCL nanofibers into the scaffold were characterized by FTIR spectroscopy. The spectra collected from PN-COL scaffolds with varying PCL concentrations and the spectra collected from pure PCL are shown in figure 3(*A*). The characteristic PCL bands are observed at 2935 cm^{-1} (asymmetric CH_2 stretching), 2862 cm^{-1} (symmetric CH_2 stretching), 1724 cm^{-1} (carbonyl stretching), 1293 cm^{-1} (C–O and C–C stretching in the crystalline phase), 1240 cm^{-1} (asymmetric COC stretching) and 1170 cm^{-1} (symmetric COC stretching) [37]. For tracking the changes in the spectra with PCL nanofiber introduction, the area under the peak at 1724 cm^{-1} was calculated. Figure 3(*A*) provides the qualitative data corresponding to PCL inclusion to the collagen matrix. The results given in figure 3(*A*) suggested that the peak associated with PCL has increased with an increase in PCL

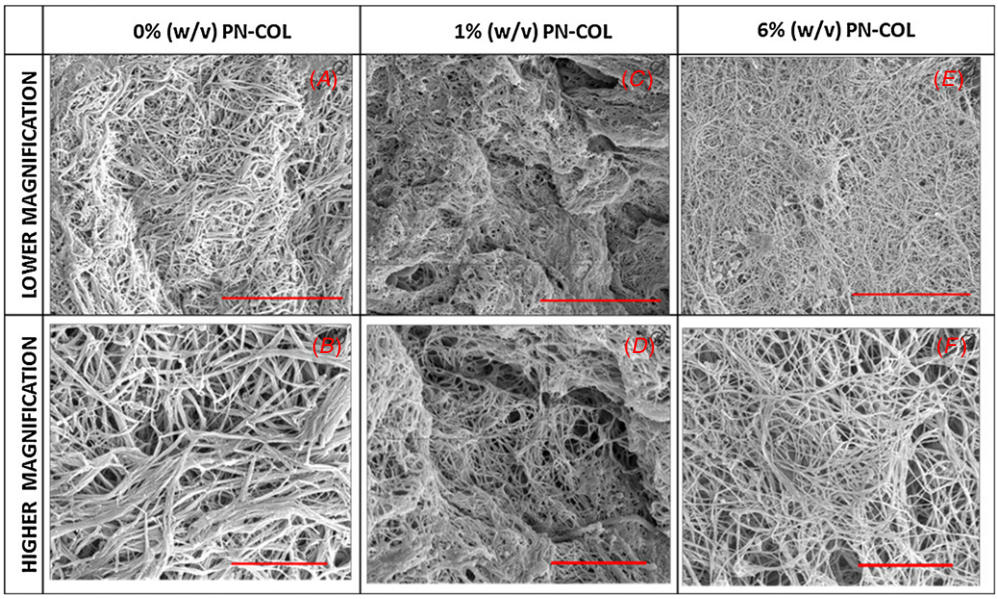

Figure 2. SEM micrographs of PN-COL scaffolds with varying PCL concentration: (*A*) and (*B*) 0% (w/v) of PN-COL scaffold taken with lower and higher magnification, (*C*) and (*D*) 1 % (w/v) of PN-COL scaffold taken with lower and higher magnification, and (*E*) and (*F*) 6% (w/v) of PN-COL scaffold taken with lower and higher magnification. For (*A*), (*C*) and (*E*), the scale bar represents 20 μm, for (*B*), (*D*) and (*F*), the scale bar represents 5 μm.

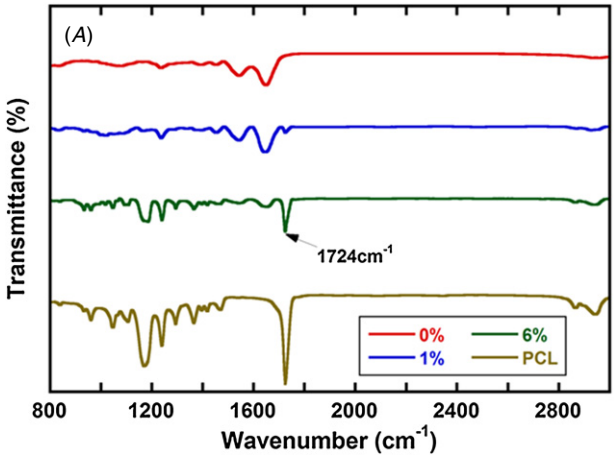

(*B*)

PCL Concentration %(w/v)	Area under the peak at 1724 cm^{-1}
0	0
1	40
6	259

Figure 3. (*A*) Traces of FTIR spectra of 0%, 1% and 6% (w/v) PN-COL scaffolds and pure PCL, and (*B*) calculations of area under the peak at 1724 cm^{-1}.

concentration within the scaffold. For instance, for 0% (w/v) PN-COL scaffolds (pure collagen scaffolds), there was no peak at 1724 cm^{-1}, while for 1% (w/v) PN-COL scaffolds the peak started to appear and for 6% (w/v) PN-COL scaffolds the peak intensity was the highest. The quantitative results with respect to changes in chemical composition (figure 3(*B*)) also suggested a similar trend. Even though these results were expected, the chemical characterization of the PN-COL scaffold was found necessary to substantiate the successful and homogenous incorporation of PCL nanofibers within collagen.

3.3. Long-term in vitro evaluation of injectable PN-COL composite scaffold

3.3.1. PCL nanofiber concentration within PN-COL scaffold mediates MC3T3-E1 cell viability and cell proliferation.

The osteocompatability data of PN-COL scaffolds at day 14 is given in figure 4. The data is given in the form of immunofluorescence images of live and dead cells within PN-COL scaffolds. The number of live cells (green labeled) was higher on 1% w/v PN-COL scaffolds (figure 4(*B*)) compared to live cells within 0% w/v PN-COL scaffolds (figure 4(*A*)). Furthermore, dead cells (red labeled) presence was lower on 1% PN-COL scaffolds compared to 0% w/v PN-COL scaffolds. The cell viability was increased with an increased PCL nanofiber concentration within the collagen scaffold. In addition, although the total number of cells within 1% (w/v) PN-COL was higher than 0% (w/v) PN-COL, the number of dead cells within 0%(w/v) PN-COL is almost the same as the counterparts within 1%(w/v) PN-COL. We were not able to take confocal images of cells within 6% (w/v) PN-COL scaffolds because a further increase of PCL presence

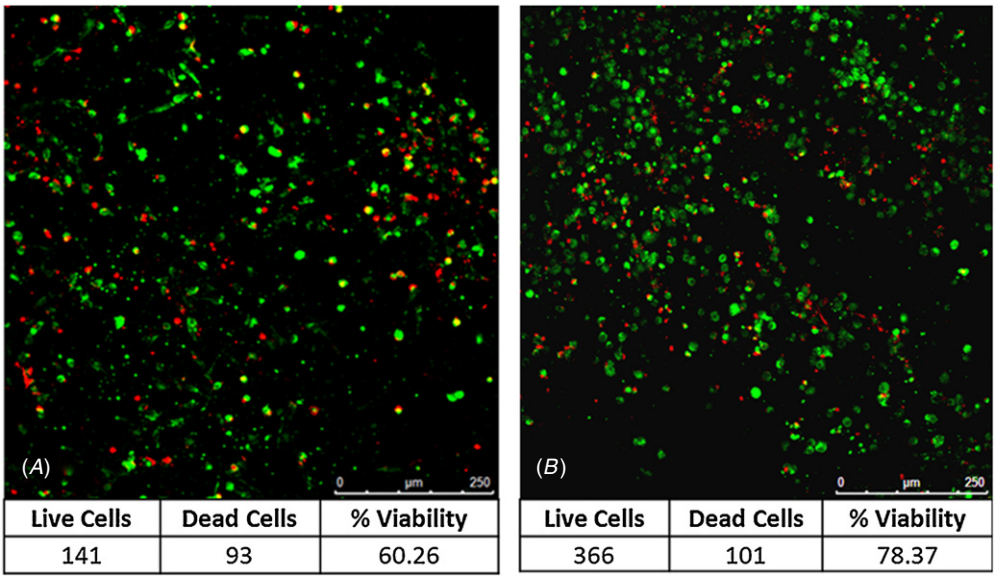

Live Cells	Dead Cells	% Viability
141	93	60.26

Live Cells	Dead Cells	% Viability
366	101	78.37

Figure 4. The qualitative and quantitative analysis of embedded cells within PN-COL scaffolds using $z = 40$ of confocal images. The live and dead MC3T3-E1 cells and their corresponding numbers (*A*) within 0% (w/v) PN-COL scaffolds and (*B*) within 1% (w/v) PN-COL scaffold at day 14. Live cells were labeled in green and dead cells were labeled in red.

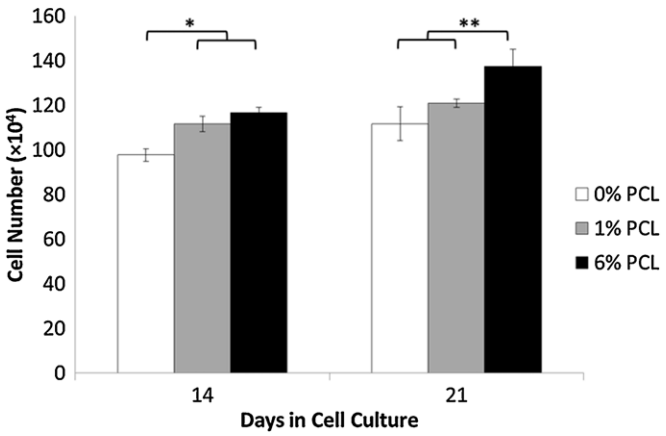

Figure 5. The MC3T3-E1 cells proliferation within PN-COL scaffold with 0% (w/v), 1% (w/v), and 6% (w/v) PCL concentration. * indicates that at day 14 cell number within 0% is significantly lower compared to 1% (w/v), and 6% (w/v) PN-COL scaffolds. ** indicates that at day 21 cell number within 6% is significantly higher compared to 1% (w/v), and 0% (w/v) PN-COL scaffolds.

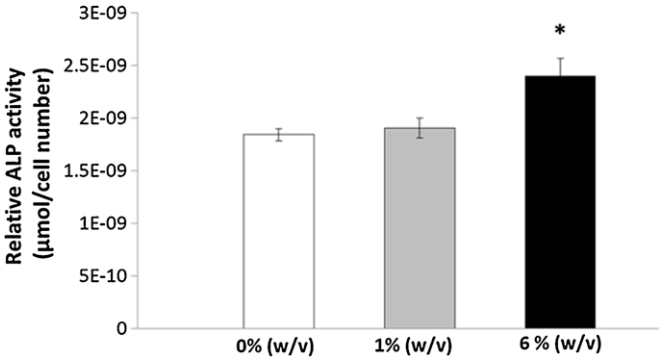

Figure 6. The alkaline phosphatase activity (ALP) of MC3T3-E1 cells within PN-COL scaffolds at day 14. (*) denotes significantly higher ALP activity compared to 1% (w/v) and 0% (w/v) scaffolds.

within the scaffold made the scaffold opaque and prevented the excitation light from passing through the samples.

MC3T3-E1 cell proliferation within PN-COL scaffolds was assessed by non-toxic aB assay. The proliferation results showed that cells were able to proliferate over 21 days within PN-COL scaffolds without showing any decrease in cell number (figure 5). At day 14, the cell number was significantly higher ($p < 0.05$) on 1% (w/v) and 6% (w/v) PN-COL scaffolds compared to collagen scaffolds (0% w/v PN-COL). At day 21, the cell number was significantly higher on 6% (w/v) PN-COL scaffolds compared to cells on 1% and 0% (w/v) PN-COL scaffolds.

3.3.2. PCL nanofiber concentration within PN-COL scaffold mediates MC3T3-E1 cells' early and later stage differentiation capacity. Alkaline phosphatase activity. The ALP is an early/intermediate osteoblastic differentiation marker. Therefore, relative ALP activity measurements of MC3T3-E1 cells within PN-COL scaffolds will identify the effect of the PCL concentration on early stage differentiation of the cells. Relative ALP activity was obtained at day 14 by dividing the amount of pNP)by the total number of cells within PN-COL scaffolds. Figure 6 shows the relative ALP activity of MC3T3-E1 cells within PN-COL scaffolds with varying PCL concentrations from 0% (w/v) to 6% (w/v). The ALP activity of cells was not different between 0% and 1% (w/v) PN-COL scaffolds. However, MC3T3-E1 cells within 6% (w/v) PN-COL scaffolds demonstrated significantly ($p < 0.05$) higher ALP activity compared to cells on 1% (w/v) PN-COL scaffolds and 0% (w/v) PN-COL scaffolds.

Calcified matrix production. The calcified matrix production was visualized and quantified to verify the extracellular matrix (ECM) mineralization as a later state of osteogenic differentiation. Figures 7(*A*)–(*D*) show SEM images (lower and higher magnification) of 0% (w/v) and

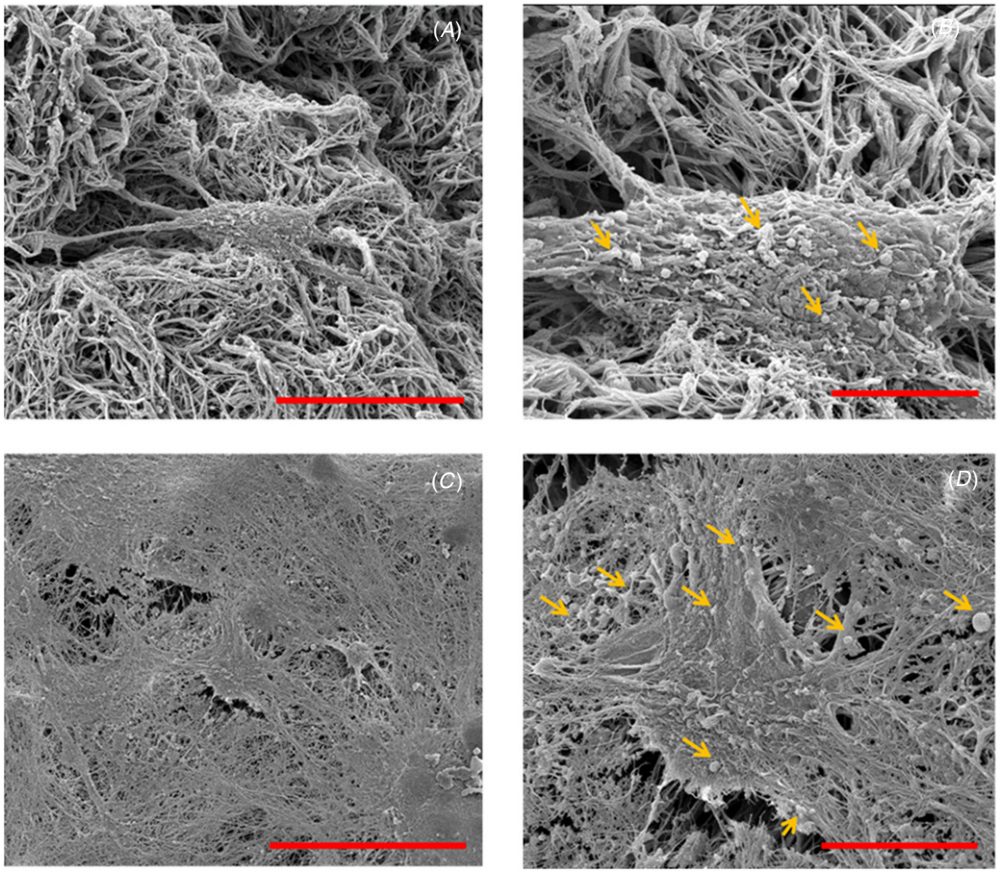

Figure 7. The SEM micrographs of mineralized matrix and cells within 6% (w/v) PN-COL and 0% (w/v) PN-COL scaffolds. (*A*) High magnification and (*B*) low magnification image of 0% (w/v) PN-COL scaffold. (*C*) High magnification and (*D*) low magnification image of 6% (w/v) PN-COL scaffold. The scale bars represent 20 μm on (*A*) and (*C*) and 10 μm on (*B*) and (*D*). Yellow arrows indicate some of the mineralized deposits around the cells.

6% (w/v) PN-COL scaffolds with a mineralized matrix and cells at day 21. The lower magnification images (figures 7(*A*) and (*C*)) of scaffolds provide information on the degree of scaffold mineralization and the position of the cells within this mineralized matrix. The higher magnification images (figures 7(*B*) and (*D*)) of scaffolds provide information on mineralized deposits on the scaffold in which some of them were pointed out with yellow arrows. The lower magnification SEM images showed that the cell layer on 6% (w/v) PN-COL scaffolds exhibited a more complex fibrillar structure and laid down more dense matrix compared to cells on 0% (w/v) scaffolds (figures 7(*A*) and (*C*)). In fact, cells within 6% (w/v) PN-COL scaffolds started to embed themselves within a deposited mineralized matrix (figure 7(*C*)) while there was a minimum matrix deposition around the cells within 0% (w/V) PN-COL scaffolds (figure 7(*A*)). The higher magnification images show the images of mineralized deposits integrated in the fibrillar matrix (figures 7(*B*) and (*D*)). In the vicinity of the cells, the ball shaped globular deposits could be distinguished. The 6% (w/v) PN-COL scaffolds had an abundance of such globular deposits compared to pure collagen scaffolds (0% PN-COL).

The mineralized matrix amount within/on PN-COL scaffolds were measured by alizarin red assay on day 14 and day 21. The quantified mineralized matrix data is given in figure 8. The results demonstrated that at day 14 there is no statistical difference in the mineralized matrix amount between

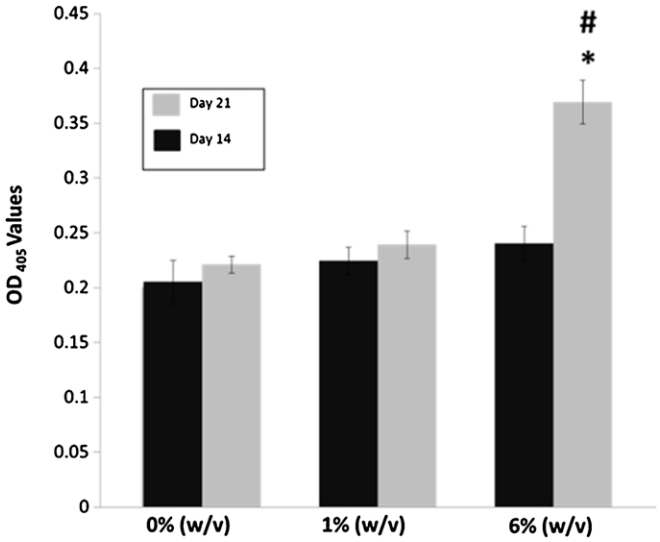

Figure 8. Mineralized matrix amount within/on PN-COL scaffolds with varying PCL concentration at day 14 and day 21. (#) denotes differences compared to the other PN-COL scaffolds ($P < 0.05$) and (*) denotes differences compared with the PN-COL scaffolds at different time points ($P < 0.05$).

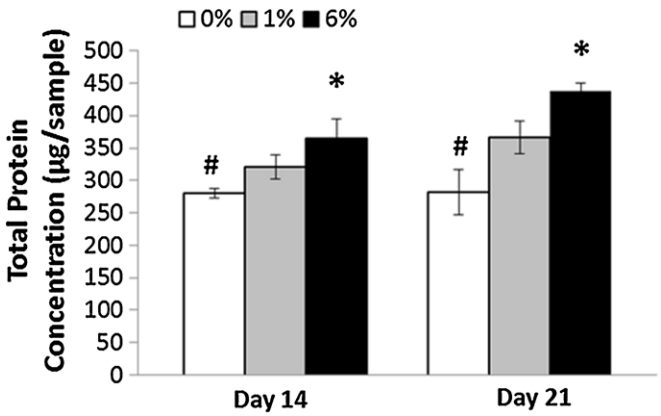

Figure 9. The total protein production of cells. (*) denotes differences compared with the PN-COL scaffolds at different time points ($P < 0.05$), (#) compared with 1% PN-COL and 6% PN-COL.

the sample groups. However, at day 21 the mineralized matrix amount is significantly ($P < 0.05$) higher on 6% (w/v) PN-COL scaffolds. This finding was also validated with SEM images (figure 7(*D*)) of scaffolds at day 21.

Total extracellular matrix protein amount. The total matrix protein production of cells on/within the scaffolds is given in figure 9. The total protein production results show that protein production on 1% (w/v) and 6% (w/v) PN-COL scaffolds are significantly higher ($p < 0.05$) than in pure collagen scaffolds on both day 14 and day 21 (figure 9). The matrix protein production is highest on 6% (w/v) PN-COL scaffolds at all the time points.

4. Discussion

In order to preserve the native structure of the collagen and to take advantage of its biological properties, the freeze drying technique and rapid prototyping technique have been used to create collagen sponges and well-defined 3D scaffolds [10, 13, 38–40] In these techniques, however, cells cannot be incorporated/encapsulated within the scaffold but can be seeded on top of the scaffold. This may raise the question of cell infiltration inside the matrix and having homogenous cell distribution throughout the scaffold. Furthermore, in electrospun collagen and collagen–polymer pre-fabricated scaffolds, the collagen sponges and well-defined 3D PCL–collagen scaffolds are not injectable and require invasive surgery to implant them to the tissue of interest. Therefore, injection of cell contained scaffolds into a bone-defect cavity using minimally invasive techniques can shift the process of cell-scaffold introduction to the body from invasive surgery to a small cutaneous incision. In this study, the advantages of injectability and biomimicry of collagen were coupled with the structural support of PCL nanofibers, to create cell encapsulated injectable 3D bone scaffolds with intricate porous internal architecture and high osteoconductivity.

For an injectable biomatrix, retention of the original volume and dimension is crucial following the injection to have successful bone regeneration. It is known that the collagen contraction due to encapsulated cells results in significant shrinkage in dimensions of a collagen construct [33, 34, 41]. Such contraction and shrinkage would negatively affect the success of the bone tissue formation because of the voids created by the shrunken matrix. Therefore, the changes in scaffolds' geometry were quantified following 14 days of cell encapsulation (figure 1). Our novel 3D collagen based injectable scaffold presented in this study was able to preserve the initial injected volume up to 95%. The 6% (w/v) PN-COL could preserve 95% of its original dimensions, while 1% (w/v) PN-COL preserved only 35% of its original volume. For pure collagen scaffolds (0% (w/v) PN-COL) the changes in size were dramatic in significance. Following the 14 days cell culture, only 25% of the scaffold size was preserved for pure collagen scaffolds. The data suggested that the preservation in dimension increased with the increased PCL nanofiber ratio inside the matrix. This can be explained by the composite nature of PN-COL scaffolds. In a pure collagen matrix, cells are anchored only on collagen fibrils and cause fibrils to contract. However, with the induction of PCL nanofibers into collagen, cells are attaching not only to these collagen fibrils but also to the PCL nanofibers. This phenomenon can be observed in SEM images of cells and the biomatrix as shown in figure 7.

It is also known that the composition of the scaffold greatly affects the cellular functions [35, 42], so homogenously incorporating PCL nanofibers into collagen was a key consideration to obtain consistent data between the sample groups in the *in vitro* study. For that reason, changes in scaffold chemistry following PCL nanofiber introduction within collagen was measured with an FTIR spectra of 0%, 1% and 6% (w/v) PN-COL scaffolds with five different locations (figure 3). The FTIR spectrum has proved that PCL nanofibers were successfully and homogenously introduced to the collagen matrix (figure 3).

The osteocompatibility and cell proliferation data on collagen and PN-COL scaffolds were obtained by aB and Live/Dead assays. The results obtained from both assays indicate good osteocompatibility and osteoconductivity for all scaffold groups. The osteocompatibility showed that the PN-COL scaffold is not toxic to the cells and further supports cell viability (figures 4(*A*) and (*B*)). The cell viability was increased with the increased PCL nanofiber concentration within the collagen scaffold. The confocal images of live and dead cells within collagen (0%) and 1% (w/v) PN-COL scaffolds showed there were higher numbers of live cells (green labeled) within PN-COL scaffolds compared to collagen scaffolds (figures 4(*A*) and (*B*)). The cell proliferation assay data (figure 5) obtained after 21 day *in vitro* culture showed that the number of embedded cells was increased with the increased PCL fraction within collagen. The 6% (w/v) PN-COL scaffolds had the highest cell number at day 21 compared 1% (w/v) PN-COL and 0% (w/v) collagen scaffolds (figure 5). The increase in cell number and viability with increased PCL concentration can be explained by the increased surface-to-volume-ratio within the scaffold after PCL nanofiber introduction. The SEM image of the (0%), 1%, and 6(w/v) PN-COL scaffolds showed that (figure 2) the

inner surface areas of the scaffolds were increased with PCL fraction within the scaffolds. This increased the surface area to provide more space for the embedded cells to attach, spread and to proliferate.

To further understand and to investigate the effect of PCL nanofibers within collagen on cellular activity, the osteogenic differentiation markers, including ALP activity, mineralization and total protein content were checked.

To identify the stage of osteoblast differentiation, the ALP activity was measured at day 14. The data (figure 6) suggested that the ALP activity was significantly ($p < 0.05$) higher at 6% (w/v) PN-COL scaffolds compared to 1% PN-COL and collagen (0% PN-COL) scaffolds. Data also showed that there is no significant difference between the ALP activities of the cells at 1% PN-COL and 0% scaffolds at day 14. The significantly higher amount of ALP activity suggests that mature osteoblast phenotype expression has started earlier on 6% (w/v) PN-COL scaffolds compared to its counterparts.

To follow the progression of differentiation, matrix mineralization and the progression of calcium deposition on/inside the scaffolds, they were quantified by Alizarin Red assay and were imaged by SEM. The SEM micrographs (figure 7) showed that cells within 6% PN-COL scaffolds had an abundance of the globular calcium deposits around them compared to 0% PN-COL (figures 7(*A*)–(*D*)). Results from the mineralization assay (figure 8) at day 21 showed that the mineralization was significantly ($p < 0.05$) higher on 6% (w/v) PN-COL scaffolds compared to its counterparts. Both quantified mineralization results (figure 8) and SEM images of mineralized matrices (figure 7) demonstrated that PCL nanofiber introduction to the collagen scaffolds positively affect the ability of cells to differentiate and calcify. Pre-osteoblast cells within 6% (w/v) PN-COL scaffolds showed an earlier onset of matrix mineralization compared to 1% (w/v) PN-COL and 0% (w/v) PN-COL scaffolds. This result can be explained with higher ALP activity of the cells within 6% (w/v) PN-COL scaffolds. The studies investigating the role of ALP in deposition of the mineralized matrix [43–45] have suggested that ALP plays a critical role in the pathway resulting in the deposition of the mineralized matrix. Our mineralization and ALP data are in agreement with these findings. The cells within 6% (w/v) PN-COL scaffolds (figure 6) showed highly expressed ALP activity compared to counterparts within 0% and 1% (w/v) PN-COL scaffolds. The higher ALP activity of cells within 6% (w/v) PN-COL scaffolds leads to accelerated mineralization within 6% (w/v) PN-COL scaffolds. The total ECM protein production results showed that protein production on 1% (w/v) and 6% (w/v) PN-COL scaffolds were significantly higher than pure collagen scaffolds and 0% (w/v) PN-COL scaffolds on both day 14 and day 21 (figure 9). The matrix protein production is highest on 6% (w/v) PN-COL scaffolds. The ECM protein production results also agreed with the proliferation and differentiation data suggesting that novel PN-COL scaffolds promote the osteoblast phenotype expression and formation of a mineralized matrix.

Conclusion

A unique, injectable and osteogenic PN-COL scaffold is introduced to the literature for the first time. The PN-COL scaffold is composed of interspersed polycaprolactone (PCL) nanofibers within pre-osteoblast cell embedded collagen type-I. In this study, the advantages of injectability and biomimicry of collagen were coupled with the structural support of PCL nanofibers. This was done to create a cell encapsulated injectable 3D bone scaffold with intricate porous internal architecture and high osteoconductivity. Our data demonstrated that the incorporation of PCL nanofibers within a collagen type-I matrix resulted in accelerated mature osteoblast phenotype development. In addition, the combination of PCL nanofibers and collagen resulted in a novel injectable scaffold with desired properties for bone tissue engineering applications, including being able to couple with cells, retain volume over an extended period of time, and having a rigid polymerized matrix without using any crosslinking agent or exothermic reaction.

Structural analysis of novel bioactive material proved that the material is chemically stable enough in an aqueous solution for an extended period of time without using crosslinking reagents and viscous enough to be injected through a syringe needle. Different to PMMA and ceramic based injectable materials, this novel scaffold can facilitate the cells within the material providing porous internal structure for cell attachment, proliferation, and differentiation. Different to current scaffolds used in bone tissue engineering including, collagen sponge, electrospun collagen and collagen–PCL mat and well-defined 3D PCL–collagen scaffolds, this novel scaffold can be injected to the body using a minimally invasive technique. In addition, during material fabrication, the control over the concentration of the collagen, the diameter of PCL nanofibers, the fraction ratio of collagen/PCL nanofibers, and the number of encapsulated cells within the scaffold provide great flexibility in the design and functionality of this novel biomatrix. PCL nanofiber inclusion within collagen positively affects the ALP activity and mineralization of encapsulated pre-osteoblast cells and supports their early osteoblast phenotype expression.

References

[1] Albrand G *et al* 2003 Independent predictors of all osteoporosis-related fractures in healthy postmenopausal women: the Ofely study *Bone* **32** 78–85
[2] Lam W M *et al* 2011 *In vitro* characterization of low modulus linoleic acid coated strontium-substituted hydroxyapatite containing PMMA bone cement *J. Biomed. Mater. Res.* B **96** 76–83
[3] Boger A *et al* 2007 Adjacent vertebral failure after vertebroplasty: a biomechanical study of low-modulus PMMA cement *Eur. Spine J.* **16** 2118–25
[4] Berlemann U and Heini P F 2002 Percutaneous cementing techniques for treatment of osteoporotic vertebral disturbances *Unfallchirurg* **105** 2–8
[5] Berlemann U *et al* 2002 Adjacent vertebral failure after vertebroplasty—a biomechanical investigation *J. Bone Joint Surg.* B **84** 748–52

[6] Ryu K S *et al* 2010 Therapeutic efficacy of injectable calcium phosphate cement in osteoporotic vertebral compression fractures: prospective nonrandomized controlled study at 6-month follow-up *World Neurosurg.* **73** 408–11

[7] Amini A A and Nair L S 2012 Injectable hydrogels for bone and cartilage repair *Biomed. Mater.* **7** 024105

[8] Noth U *et al* 2010 Cell delivery therapeutics for musculoskeletal regeneration *Adv. Drug Deliv. Rev.* **62** 765–83

[9] Hesse E *et al* 2010 Collagen type I hydrogel allows migration, proliferation, and osteogenic differentiation of rat bone marrow stromal cells *J. Biomed. Mater. Res.* A **94** 442–9

[10] Oliveira S M *et al* 2010 An improved collagen scaffold for skeletal regeneration *J. Biomed. Mater. Res.* A **94** 371–9

[11] Xiao Y *et al* 2003 Tissue engineering for bone regeneration using differentiated alveolar bone cells in collagen scaffolds *Tissue Eng.* **9** 1167–77

[12] Gee A O *et al* 2012 Fabrication and evaluation of biomimetic-synthetic nanofibrous composites for soft tissue regeneration *Cell Tissue Res.* **347** 803–13

[13] Lee H *et al* 2011 Designed hybrid scaffolds consisting of polycaprolactone microstrands and electrospun collagen-nanofibers for bone tissue regeneration *J. Biomed. Mater. Res.* B **97** 263–70

[14] Yildirim E D *et al* 2011 Enhanced cellular functions on polycaprolactone tissue scaffolds by O_2 plasma surface modification *Plasma Process. Polym.* **8** 256–67

[15] Burg K J L, Porter S and Kellam J F 2000 Biomaterial developments for bone tissue engineering *Biomaterials* **21** 2347–59

[16] Yildirim E D *et al* 2010 Accelerated differentiation of osteoblast cells on polycaprolactone scaffolds driven by a combined effect of protein coating and plasma modification *Biofabrication* **2** 014109

[17] Lee J J *et al* 2009 Nanofibrous membrane of collagen-polycaprolactone for cell growth and tissue regeneration *J. Mater. Sci.-Mater. Med.* **20** 1927–35

[18] Ahn S *et al* 2012 A new hybrid scaffold constructed of solid freeform-fabricated PCL struts and collagen struts for bone tissue regeneration: fabrication, mechanical properties, and cellular activity *J. Mater. Chem.* **22** 15901–9

[19] Zeugolis D I *et al* 2008 Electro-spinning of pure collagen nano-fibres—just an expensive way to make gelatin? *Biomaterials* **29** 2293–305

[20] Rho K S *et al* 2006 Electrospinning of collagen nanofibers: effects on the behavior of normal human keratinocytes and early-stage wound healing *Biomaterials* **27** 1452–61

[21] Buttafoco L *et al* 2006 Electrospinning of collagen and elastin for tissue engineering applications *Biomaterials* **27** 724–34

[22] Kidoaki S, Kwon I K and Matsuda T 2005 Mesoscopic spatial designs of nano- and microfiber meshes for tissue-engineering matrix and scaffold based on newly devised multilayering and mixing electrospinning techniques *Biomaterials* **26** 37–46

[23] Telemeco T A *et al* 2005 Regulation of cellular infiltration into tissue engineering scaffolds composed of submicron diameter fibrils produced by electrospinning *Acta Biomater.* **1** 377–85

[24] Zhang Y Z *et al* 2005 Characterization of the surface biocompatibility of the electrospun PCL-collagen nanofibers using fibroblasts *Biomacromolecules* **6** 2583–9

[25] Zhong S P *et al* 2007 Development of a novel collagen-GAG nanofibrous scaffold via electrospinning *Mater. Sci. Eng.* C **27** 262–6

[26] Yang L *et al* 2008 Mechanical properties of single electrospun collagen type I fibers *Biomaterials* **29** 955–62

[27] Li M Y *et al* 2005 Electrospun protein fibers as matrices for tissue engineering *Biomaterials* **26** 5999–6008

[28] Matthews J A *et al* 2002 Electrospinning of collagen nanofibers *Biomacromolecules* **3** 232–8

[29] Reichert J C *et al* 2009 Fabrication of polycaprolactone collagen hydrogel constructs seeded with mesenchymal stem cells for bone regeneration *Biomed. Mater.* **4** 065001

[30] Sung K E *et al* 2009 Control of 3-dimensional collagen matrix polymerization for reproducible human mammary fibroblast cell culture in microfluidic devices *Biomaterials* **30** 4833–41

[31] Kreger S T *et al* 2010 Polymerization and matrix physical properties as important design considerations for soluble collagen formulations *Biopolymers* **93** 690–707

[32] Su G N C *et al* 2003 *In situ* collagen gelation: a new method for constructing large tissue in rotary culture vessels *In vitro Cell. Dev. Biol. Anim.* **39** 368–74

[33] Chieh H F *et al* 2010 Effects of cell concentration and collagen concentration on contraction kinetics and mechanical properties in a bone marrow stromal cell-collagen construct *J. Biomed. Mater. Res.* A **93** 1132–9

[34] Nillesen S T M *et al* 2011 Design and *in vivo* evaluation of a molecularly defined acellular skin construct: reduction of early contraction and increase in early blood vessel formation *Acta Biomater.* **7** 1063–71

[35] Sundelacruz S and Kaplan D L 2009 Stem cell- and scaffold-based tissue engineering approaches to osteochondral regenerative medicine *Semin. Cell Dev. Biol.* **20** 646–55

[36] Mesquita P, de Sousa Gomes P, Sampaio P, Juodzbalys G, Afonso A and Fernandes M H 2012 Surface properties and osteoblastic cytocompatibility of two blasted and acid-etched titanium implant systems with distinct microtopography *J. Oral Maxillofac. Res.* **3** e4

[37] Wang J, Cheung M K and Mi Y L 2002 Miscibility and morphology in crystalline/amorphous blends of poly(caprolactone)/poly(4-vinylphenol) as studied by DSC, FTIR, and C-13 solid state *NMR Polymer* **43** 1357–64

[38] Yang H S *et al* 2012 Comparison between heparin-conjugated fibrin and collagen sponge as bone morphogenetic protein-2 carriers for bone regeneration *Exp. Mol. Med.* **44** 350–5

[39] Yoshida T *et al* 2010 Osteogenic activity of MG63 cells on bone-like hydroxyapatite/collagen nanocomposite sponges *J. Mater. Sci.-Mater. Med.* **21** 1263–72

[40] Muller W E G *et al* 2009 Sponge spicules as blueprints for the biofabrication of inorganic–organic composites and biomaterials *Appl. Microbiol. Biotechnol.* **83** 397–413

[41] Nagakura T *et al* 2005 Effect of viscous injectable pure alginate sol on cultured fibroblasts *Plast. Reconstr. Surg.* **116** 831–8

[42] Khan Y *et al* 2008 Tissue engineering of bone: material and matrix considerations *J. Bone Joint Surg. Am.* **90** 36–42

[43] Porter J R, Henson A and Popat K C 2009 Biodegradable poly(epsilon-caprolactone) nanowires for bone tissue engineering applications *Biomaterials* **30** 780–8

[44] Storrie H and Stupp S I 2005 Cellular response to zinc-containing organoapatite: an *in vitro* study of proliferation, alkaline phosphatase activity and biomineralization *Biomaterials* **26** 5492–9

[45] Anderson H C 1995 Molecular-biology of matrix vesicles *Clin. Orthop. Relat. Res.* **314** 266–80